catalysts

MDPI

Article

Glucose Isomerization to Fructose Catalyzed by MgZr Mixed Oxides in Aqueous Solution

Xiongxiong Zuo and Xing Tang *

Xiamen Key Laboratory of Clean and High-Valued Applications for Biomass, Fujian Engineering and Research Center of Clean and High-Valued Technologies for Biomass, College of Energy, Xiamen University, Xiang'an South Road, Xiamen 361102, China

* Correspondence: x.tang@xmu.edu.cn

Abstract: The catalytic isomerization of glucose to fructose plays a pivotal role in the application of biomass as a feedstock for chemicals. Herein, we propose a facile solid-state-grinding strategy to construct ZrO_2/MgO mixed oxides, which offered an excellent fructose yield of over 34.55% and a high selectivity of 80.52% (80 °C, 2 h). The co-mingling of amphiphilic ZrO_2 with MgO improved the unfavorable moderate/strongly basic site distribution on MgO, which can prohibit the side reactions during the reaction and enhance the fructose selectivity. Based on the catalyst characterizations, MgO was deposited on the ZrO_2 surface by plugging the pores, and the addition of ZrO_2 lessened the quantity of strongly basic sites of MgO. Additionally, the presence of ZrO_2 largely enhanced the catalyst stability in comparison with pure MgO by recycling experiments.

Keywords: glucose isomerization; fructose; MgO; ZrO_2

1. Introduction

The use of non-renewable fossil resources has caused environmental damage and raised concerns about environmental sustainability, and the renewable biomass resource as the potential alternative to fossil resources is recently gaining momentum [1–3]. In biomass refining, 5-hydroxymethylfurfural (HMF), touted as a versatile biomass-derived platform molecule for the production of value-added chemicals, polymeric materials and liquid fuels, can be derived from the catalytic conversion of glucose and fructose [4–6]. Glucose can be obtained by the enzymatic hydrolysis of polysaccharide macromolecule cellulose, which is widely found in nature and is abundant and easy to obtain [7,8]. The conversion of glucose to HMF is much more difficult than fructose, although they are isomers of each other [9–11]. In addition, fructose is widely used to make sweeteners, preservatives, diabetic drugs and so on, and it is considered to be a key intermediate compound [12,13]. Therefore, the isomerization of glucose to fructose is a crucial intermediary step in the use of biomass as a feedstock for chemicals.

Currently, industrial production of high fructose corn syrup is catalyzed by immobilized glucose isomerase, but there are still problems, such as the need for more stringent reaction conditions (lower temperatures, narrow pH operating window) for glucose isomerase activity. In addition, from an economic point of view, a large number of enzymes are required to improve the efficiency of enzymatic isomerization, which increases the cost of investment [14]. Also, for this reason, many homogeneous and solid catalysts have been developed for the conversion of aldehydes and ketones [15–17]. For example, the isomerization of glucose (4.0 wt%) could proceed in a $NaAlO_2$ aqueous solution at 80 °C for 30 min, which offered a fructose yield of 25% with a poor selectivity of less than 29%. Nguyen et al. investigated the catalytic glucose ketonization with metal chlorides (Cr^{3+}, Al^{3+}, Ga^{3+}) as Lewis acid catalysts, and a fructose yield of 15–18% was obtained [18,19]. The lower fructose yields achieved by the above homogeneous catalytic systems and their non-

check for updates

Citation: Zuo, X.; Tang, X. Glucose Isomerization to Fructose Catalyzed by MgZr Mixed Oxides in Aqueous Solution. *Catalysts* **2024**, *14*, 332. https://doi.org/10.3390/catal14050332

Received: 6 May 2024
Revised: 16 May 2024
Accepted: 17 May 2024
Published: 18 May 2024

recyclability and high substrate concentration requirements have rendered homogeneous catalyzed glucose isomerization unsatisfactory for research purposes [15].

Comparatively, in recent years, solid catalysts, especially alkaline earth metal oxides, have been applied to aldose ketonization, which can be well separated and reused and can be doped and modified to improve their catalytic activity [20]. Naturally occurring metal oxides (zirconium oxide, magnesium oxide, calcium oxide, titanium dioxide and cerium dioxide) are popular due to their inherent acid–base favorable properties, and magnesium-based metal oxides are currently showing better catalytic properties for glucose isomerization [21,22]. Marianou et al. prepared magnesium oxide (with a small amount of calcium oxide) calcined from purely natural magnesite, which could give a fructose yield of 33.4% with a selectivity of 75.8% from glucose at 90 °C for 45 min via a proton transfer mechanism [23]. In addition, a series of magnesium-based composite metal oxides have good catalytic activity for glucose isomerization. For instance, Rabee et al. prepared magnesium–zirconium composite metal oxides with different ratios by calcining magnesium-zirconium hydrotalcite, which offered a fructose yield close to 30% with a selectivity of 74% at 95 °C for 3 h [24]. Similarly, Mahala et al. found that amphoteric zinc oxide is able to modulate the acidity and base of the magnesium–zinc composite oxides, giving a fructose yield of 30 wt% with a selectivity of nearly 80 wt% [25]. Although these magnesium-based metal oxides have achieved better catalytic activity, they are more cumbersome and time-consuming to prepare. Interestingly, pure ZrO_2 was previously reported to catalyze glucose isomerization and gave only a 15% fructose yield due to the presence of its basic active center [26].

Considering the stability, low cost and suitability of metal complex oxides for the ketonization of glucose to fructose, in this study, a facile complex metal oxide preparation method was developed, which was made by mixing magnesium and zirconium nitrates by thorough milling and calcination in air. The aqueous-phase catalysis of glucose with appropriate proportions of magnesium and zirconium mixed oxides gave 34.55 wt% fructose yield and up to 80 wt% selectivity under milder reaction conditions.

2. Results and Discussion

2.1. Characterization of the Synthesized MgO/ZrO_2 Catalysts

The morphology and crystalline phase of pristine metal oxides (zirconia and magnesium oxide) and composite metal oxides (Mg/Zr-0.5, Mg/Zr-1.0, Mg/Zr-2.0) were investigated by X-ray diffraction (XRD) (Figure 1). Upon comparing with the original zirconia comparison cards JCPDS:88-1007 and 78-0047, it is observed that zirconia exhibits both tetragonal and monoclinic phases. Moreover, the tetragonal phase predominantly manifests within the composite oxide catalyst [27]. The (111), (200) and (220) crystal planes of magnesium oxide displayed distinct diffraction peaks at 35.7°, 42.3° and 61.8°, respectively. Furthermore, the composites exhibited significant fusion effects [28]. It has been noted that in the composites, the diffraction peaks of zirconia corresponding to (101) and (112) crystal faces undergo a discernible shift towards higher 2θ angles. Additionally, these diffraction peaks appear broader, suggesting the incorporation of magnesium atoms into the zirconia lattice [25,29,30].

Scanning electron microscopy-energy spectrometry was utilized to estimate the elemental content distribution on the catalyst surface, with the findings presented in Table 1. The surface Mg/Zr atomic ratio exceeds the theoretical Mg/Zr atomic ratio.

The morphology of the prepared oxide catalysts was observed using scanning electron microscopy, as shown in Figure 2. Figure 2a,b illustrate that pure zirconia forms irregular aggregates, and pure magnesium oxide exhibits a lamellar structure. As the magnesium content in the mixed catalyst is gradually doubled compared to the zirconium molar equivalents (Figure 2c,d), distinct flakes of magnesium oxide become visible, adhering to the bulk on the catalyst surface. With further increases in magnesium content, a significant aggregation of magnesium flakes occurs, rendering the catalyst surface noticeably rougher. It is observed that magnesium oxide covers the ZrO_2 surface in the form of flakes, resulting in

the Mg/Zr atomic ratio on the surface exceeding the theoretical value (Table 1). Specifically, surface Mg/Zr atomic ratios estimated by XPS were much higher than those acquired by SEM-EDX due to the narrower testing depth of XPS (2–10 nm) compared to SEM-EDX, consistent with earlier elemental analyses. In addition, examination of the elemental face-scan images in Figure 3 reveals uniform dispersion of Mg, Zr and O elements.

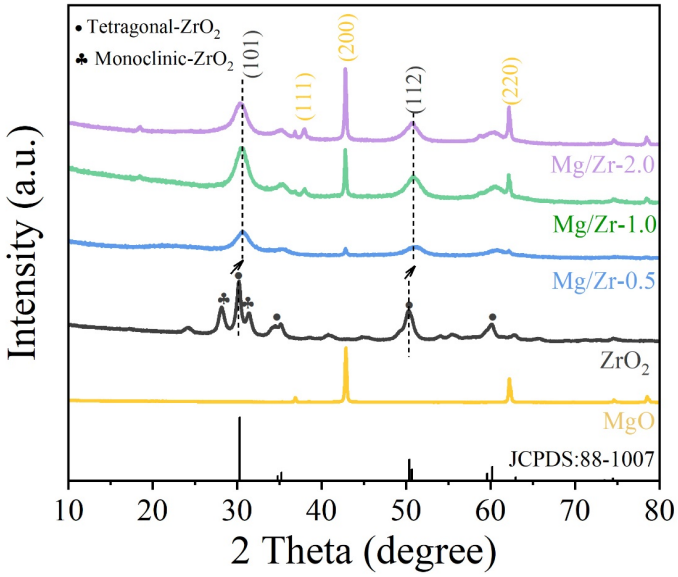

Figure 1. XRD profiles of synthesized catalysts and pure oxides.

Table 1. Nominal and actual surface Mg/Zr atomic ratios of catalysts.

Catalyst	Nominal Surface Mg/Zr Atomic Ratios	Actual Surface Mg/Zr Atomic Ratios
Mg/Zr-0.5	0.50	0.84 [a] (3.43) [b]
Mg/Zr-1.0	1.00	3.76 [a] (7.78) [b]
Mg/Zr-2.0	2.00	17.59 [a] (64.65) [b]

[a] Estimated by SEM-EDX. [b] Estimated by XPS.

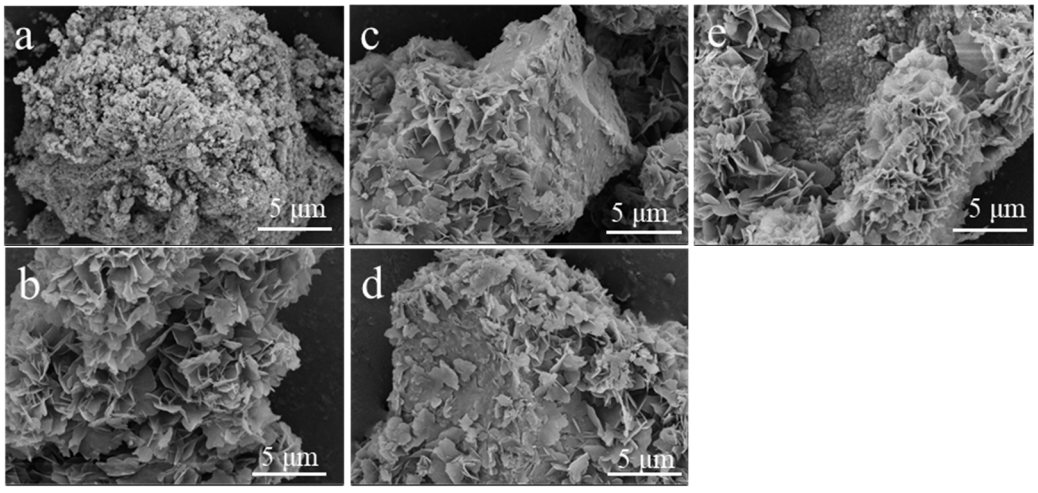

Figure 2. SEM images of (**a**) ZrO_2, (**b**) MgO, (**c**) Mg/Zr-0.5, (**d**) Mg/Zr-1.0, (**e**) Mg/Zr-2.0.

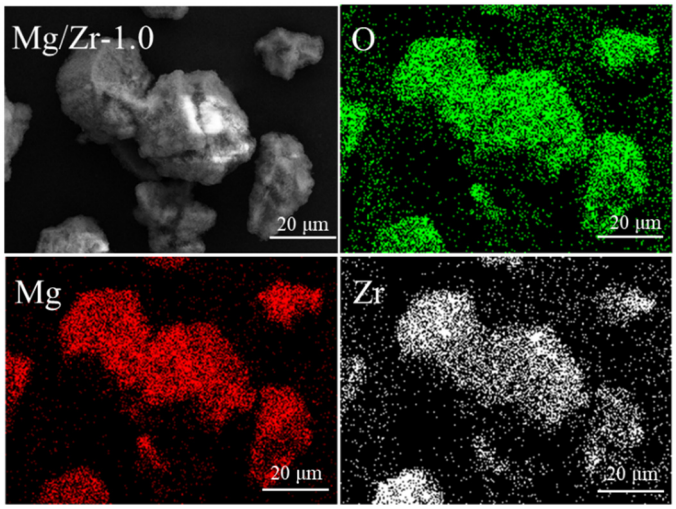

Figure 3. Element face mapping of Mg/Zr-1.0.

The results from the N_2 adsorption–desorption isotherms (Figure 4) indicated that all samples exhibited typical type IV isotherms, indicative of mesoporous materials. The BET-specific surface area, pore volume and average pore size distribution of each oxide catalyst are shown in Table 2. The average pore size and pore volume of the composite oxides declined significantly after the addition of magnesium oxide, likely due to the coating of magnesium oxide on the outer surface of zirconia while leaving the inner channel intact. Moreover, the addition of magnesium oxide did not obviously impact the specific surface area of composite metal oxides (Table 2).

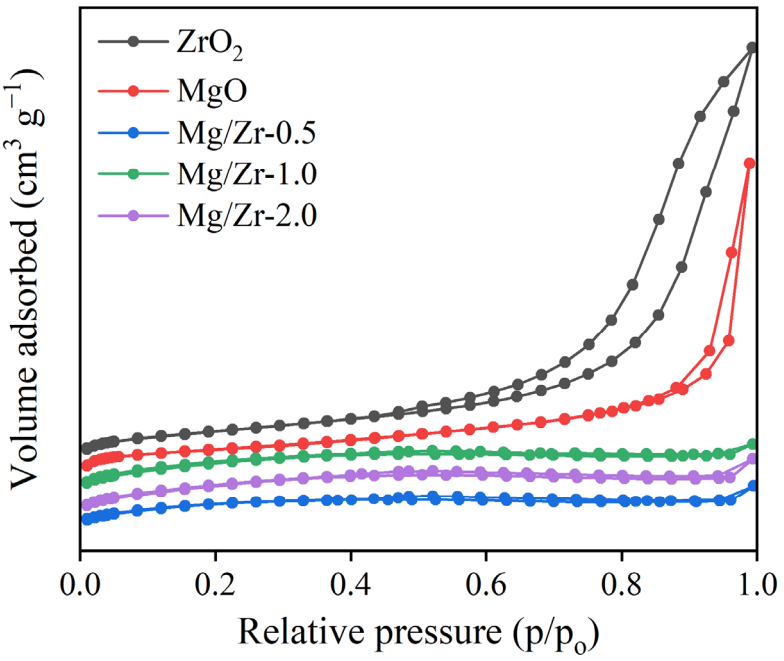

Figure 4. N_2 adsorption–desorption isotherms of synthesized catalysts and pure oxides.

XPS test results indicate the presence of zirconium, oxygen and magnesium on the Mg/Zr-1.0 surface. Figure 5 shows the XPS spectra of the electronic binding energies of Zr 3d, Mg 1s and O 1s for ZrO_2, MgO and Mg/Zr-1.0. It can be observed that Zr and Mg in Mg/Zr-1.0 exist in the Zr^{4+} oxidation state (181.78 and 183.98 eV) (Figure 5a) and Mg^{2+} oxidation state (1304.18 eV) (Figure 5b), respectively [31]. The O 1s signal of Mg/Zr-1.0 is deconvoluted into three components: the Mg-O (530.0 eV), Mg-OH (530.7 eV), and H_2O

(533.4 eV) [32,33]. However, O^{2-} species in ZrO_2 did not appear in the O 1s of Mg/Zr-1.0. As mentioned above, the catalyst surface is mainly coated by magnesium oxide. In addition, it can be seen from the O 1s spectra of MgO that the area of the Mg-OH peak is larger than that of the MgO lattice oxygen (Mg-O) form, which suggests that MgO has strong basicity and is prone to adsorb water molecules in the environment to form hydroxide species. In the Mg/Zr-1.0 sample, the peak areas of these two oxygen species occupy the opposite situation, which indicates that the introduction of Zr into MgO weakened its surface alkalinity and elevated the content of lattice oxygen species on the catalyst surface.

Table 2. Physical characteristics of the prepared metal oxide catalysts.

Catalyst	Specific Surface Area (m^2/g) [a]	Pore Volume (cm^3/g) [a]	Average Pore Diameter (nm) [a]	Strong Basic Sites (μmol/g) [b]	Ratio of Moderate/Weak Basic Sites to Strong Basic Sites
ZrO_2	46.7	0.185	15.2	0.0	--
MgO	31.6	0.136	17.1	96.2	2.3
Mg/Zr-0.5	40.7	0.022	2.1	34.4	3.2
Mg/Zr-1.0	49.6	0.028	2.2	45.1	3.5
Mg/Zr-2.0	45.0	0.035	3.1	63.5	2.7

[a] Determined by N_2 adsorption isotherm. [b] Estimated by the CO_2-TPD profiles.

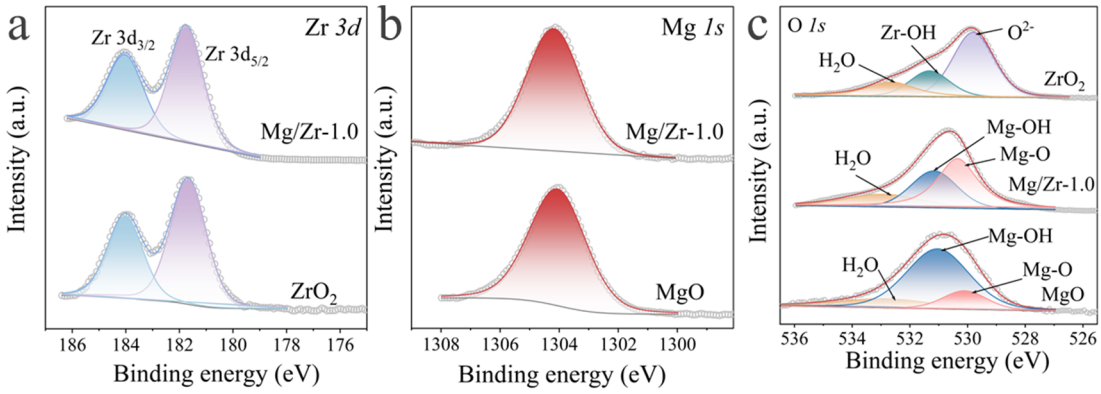

Figure 5. XPS spectra of (**a**) Zr 3d, (**b**) Mg 1s, and (**c**) O 1s of MgO, ZrO_2, and Mg/Zr-1.0.

The CO_2-TPD measurements were conducted with the aim of determining the entirety of alkalinity (as outlined in Table 2) and the distribution of the alkali strength of the prepared oxide catalysts. As shown in Figure 6, all samples show two major CO_2 desorption peaks in the range of 200–450 °C, attributed to weak/medium basic centers and strong basic centers, respectively [34]. MgO has two desorption peaks at 325 °C (moderately basic site) and 394 °C (strongly basic site). With the reduction of the Mg/Zr atomic ratio, the intensity of the desorption peak becomes lower and the center moves towards the low temperature at 276 °C and 330 °C, respectively. This can be attributed to the decrease in the desorption amount of CO_2 with increasing Zr content. As shown in Table 2, the strong basic center of the catalyst dramatically decreased from 96 to 34 μmol/g with the decline in the Mg/Zr atomic ratio, which may be due to the doping of amphoteric zirconia [35], which correspondingly weakened the influence of the strong basic center. Moreover, the catalyst Mg/Zr-1.0 showed the largest ratio of weakly and moderately basic sites to strongly basic sites (3.5), suggesting that the doping of a moderate amount of zirconia enhanced the ratio of weakly and moderately basic sites and thus improved the catalytic activity.

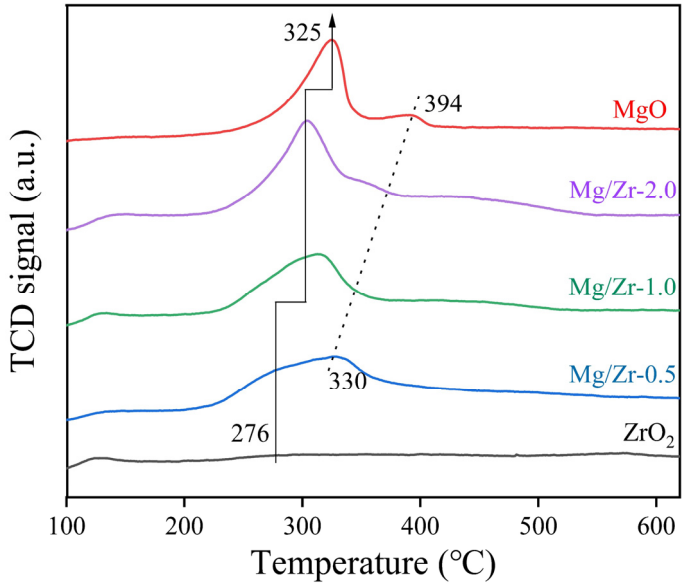

Figure 6. CO_2-TPD profiles of synthesized catalysts and pure oxides.

Figure 7 displays the FT-IR spectra of MgO-, ZrO_2- and MgZr-mixed metal oxide catalysts. The FTIR spectra of the MgZr samples with different ratios have a distinct band from 3400 to 3660 cm^{-1}, which accounted for the -OH stretching vibration induced by the water molecules adsorbed on the catalyst surface [36]. However, in pure MgO and MgZr samples at higher Mg/Zr ratios, the band at 3696 cm^{-1} may be ascribed to the OH-groups exposed to the magnesium catalyst [37]. The nature of the alkaline center was reportedly assessed using the splitting value of the υ3OCO vibrations (Δυ3) by Rabee et al. [24]. The 1519 and 1423 cm^{-1} (Δυ3 = 96 cm^{-1} < 100 cm^{-1}) bands appearing in Mg-containing samples may represent monodentate carbonate species [38]. The formation of monodentate carbonates requires the presence of surface-coordinated unsaturated O^{2-} centers [24,39]. Thus, FTIR spectra indicate that the predominant active sites on the surface of the Mg-containing catalysts are the coordinated unsaturated Lewis base sites (cu-O^{2-}).

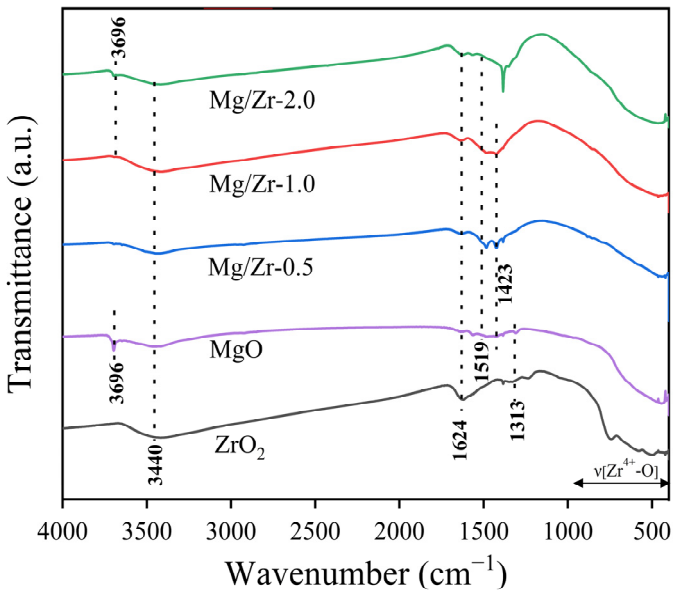

Figure 7. FTIR spectra of synthesized catalysts and pure oxides.

2.2. Catalytic Evaluation of Different MgO-Based Mixed Oxide on Glucose Isomerization

Mixed metal oxides with a molar ratio of 1 were prepared in the same way with different metal salts, and the prepared catalysts were screened under identical reaction conditions; the results are shown in Table 3. It can be seen that the fructose yields obtained through the doping of other oxides are all within 20–30%. Among them, the admixture of CaO considerably improved glucose conversion, thus leading to poor fructose selectivity (less than 40%). In addition, the blending of Sn and Zn, both amphoteric metals, into MgO showed better fructose selectivity (79.66% and 85.92%, respectively), yet the fructose yields were lower than 30%, which was not as effective as that of Mg/Zr-1.0. It can be concluded that Mg/Zr-mixed oxides showed the best catalytic performance.

Table 3. Isomerization of glucose to fructose over different metal oxide catalysts.

Entry	Catalyst	Glucose Conv. (%)	Fructose Yield. (%)	Fructose Selectivity (%)
1	Mg/Al-1.0	36.45	20.61	56.54
2	Mg/Sn-1.0	35.75	28.48	79.66
3	Mg/Zn-1.0	30.77	26.44	85.92
4	Mg/Ca-1.0	55.54	21.74	39.14
5	Mg/Mn-1.0	35.23	22.01	62.47
6	Mg/Zr-1.0	42.90	34.55	80.52
7	MgO	40.86	27.08	66.28

Conditions: 1 mmol glucose, 6 mL H_2O, 2 h, 80 °C.

Figure 8 summarizes the catalytic activity results for the isomerization of glucose to fructose over ZrO_2, MgO, and Mg/Zr mixed metal oxide catalysts. It is important to note that no detectable mannose was observed in any of the reactions, indicating that no discernible differential isomerization of glucose took place under the experimental conditions in this study [40]. It has been reported that in base-catalyzed glucose isomerization reactions, either very little mannose is formed or mannose consistently appears as a minor product [41,42]. Initially, the impact of the Mg/Zr atomic ratio was examined while ensuring consistency in other reaction parameters (3 wt% glucose, 80 °C, 9 h).

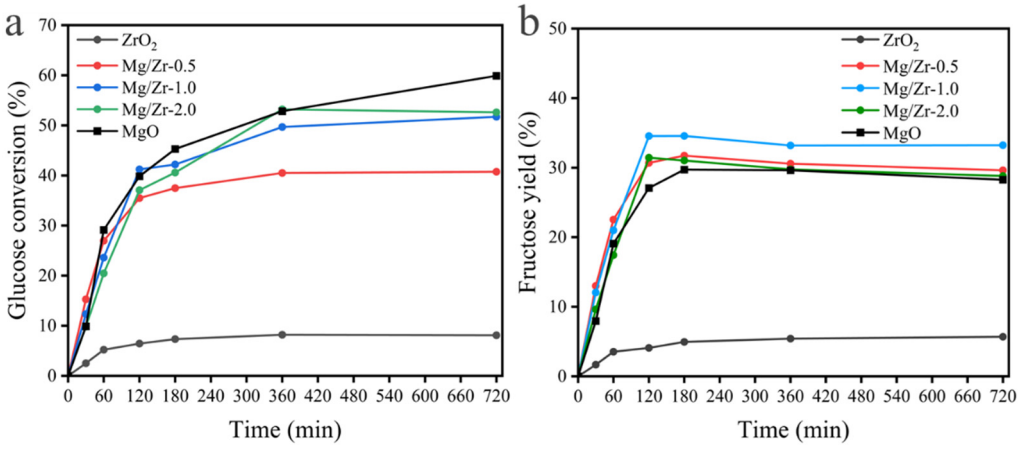

Figure 8. Effect of catalysts with different Mg/Zr ratios on glucose isomerization of fructose: (**a**) glucose conversion and (**b**) fructose yield. Reaction conditions: 1 mmol glucose, 6 mL H_2O, 80 °C.

Figure 8 illustrates the time course of glucose isomerization. As shown in Figure 8a, the MgO-catalyzed conversion of glucose showed a continuously growing trend within 9 h. Other catalysts behave more. Similarly, the glucose conversions attained by them increased with the extension of reaction time until 180 min, after which they gradually plateau with a further extension of the reaction time. As shown in Figure 8b, the yield of fructose obtained from the prepared catalysts showed a more consistent performance.

The highest fructose yield was reached when the reaction was conducted for a duration of 3 h, and it began to show a slight decline when the time was prolonged. The reduced yield of fructose may be caused by side reactions of fructose that lead to degradation or polymerization to form by-products such as humin [43,44]. The yield of fructose obtained with MgO was almost 20% higher than that of ZrO_2 under the same reaction conditions, but it displayed the highest glucose conversion (>60%) at 9 h of reaction, which led to a poorer fructose selectivity (less than 50%). This could be attributed to the higher concentration of strongly basic sites inherent to MgO itself [45,46]. Although the pristine ZrO_2 gave a lower fructose yield, its incorporation into magnesium oxide exhibited higher fructose yields than MgO. With the increase in zirconium oxide, when the Mg/Zr ratio reached 1.0, the glucose conversion finally increased considerably to 51.71%, and the fructose yield and selectivity reached 34.57% and 66.85%, respectively. Therefore, it can be hypothesized that the increase in zirconia doping weakens the strong basic sites inherent in MgO, thereby increasing the catalytic activity [47].

2.3. Influence of Other Reaction Parameters

Based on the excellent catalytic activity of Mg/Zr-1.0 for glucose isomerization, the effect of other parameters, namely, reaction temperature, catalyst dosage and substrate concentration, was further investigated. Figure 9 illustrates the isomerization of glucose in the temperature range of 80–110 °C. When the reaction is carried out for 2 h, the rate of glucose conversion is going to grow as the temperature of the reaction increases. The time required to achieve the same glucose conversion at different temperatures decreases with rising temperature, indicating that the higher the temperature, the faster the glucose consumption. As can be seen from Figure 9b, the fructose yields at different temperatures were stabilized at a certain value at the end with the extension of time, and the fructose yields were all in the range of 30–35% at 2 h of reaction. However, glucose conversion is preferable at high temperatures, so the fructose selectivity is correspondingly poor. This suggests that an increase in temperature not only accelerates the conversion of the substrate but also results in the side reactions of glucose or fructose [48]. The above results showed that the Mg/Zr-1.0 catalyst could give a desirable fructose yield with a relatively high selectivity at 80 °C.

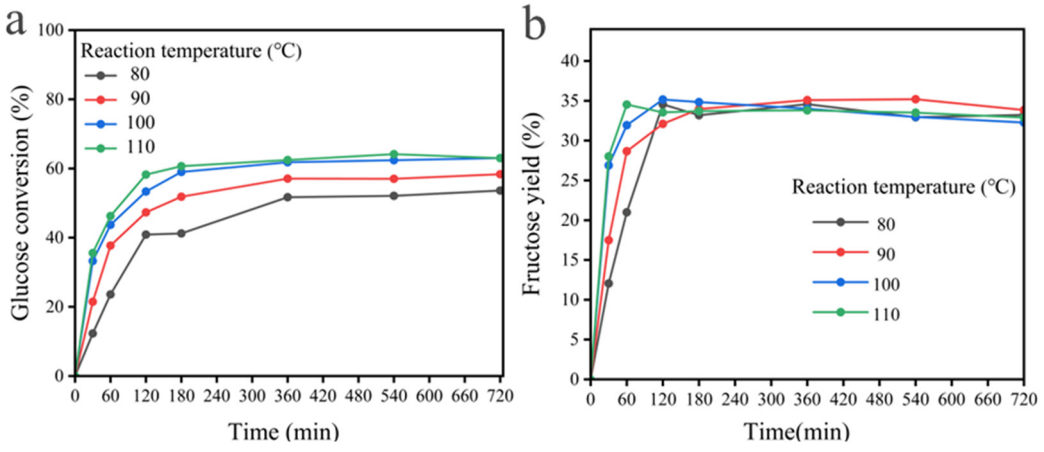

Figure 9. Effect of temperature on glucose isomerization: time-dependent progression of the reaction for glucose conversion (**a**) and fructose yield (**b**) at various reaction temperatures was investigated using the Mg/Zr-1.0 catalyst. Reaction conditions included 1 mmol glucose, 6 mL H_2O, and 0.02 g catalysts.

We further investigated the effect of the ratio of catalyst dosage to substrate dosage on the catalytic isomerization of glucose. The results of the effect of catalyst dosage adjustment on the reaction are shown in Figure 10. It can be seen that the increase in glucose conversion becomes apparent as the ratio of substrate to catalyst dosage declines. This is because the increment of catalyst dosage promotes collisional contact with glucose molecules and can

provide more active sites to participate in the reaction [49]. When the reaction proceeded for a duration of 3 h, in terms of fructose yield, when the ratio of substrate to catalyst mass was decreased from 18 to 9, the fructose yield enhanced by 5% to reach a maximum value of 34.55%, followed by a further decrease in the ratio and a drop in the fructose yield. Although the fructose yield at the end of the reaction with the smallest substrate-to-catalyst ratio (1.8) was comparable to that at a ratio of 9, it had a higher glucose conversion, resulting in somewhat inferior fructose selectivity. This confirms that the appropriate amount of catalyst is sufficient to catalyze the conversion of the substrate, whereas an excessive amount of catalyst can initiate unwanted side reactions.

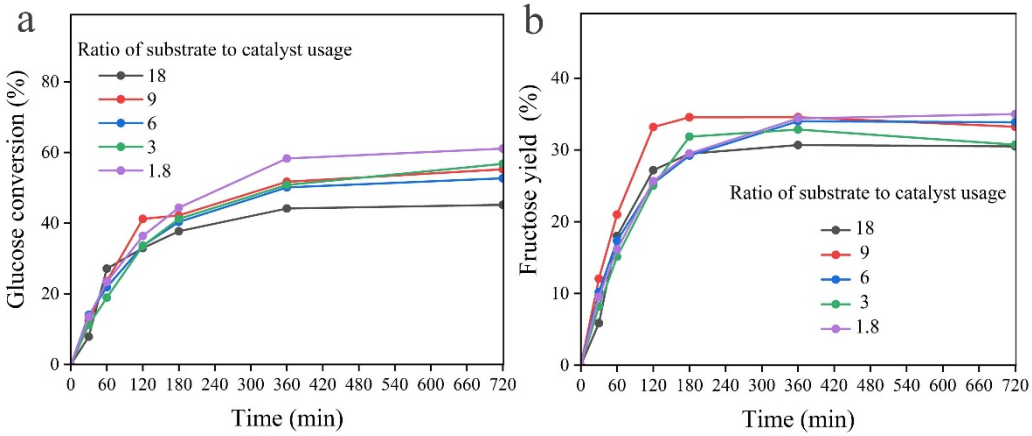

Figure 10. Comparative results of glucose isomerization: time-dependent progression of the reaction for glucose conversion (**a**) and fructose yield (**b**) at different ratios of substrate to catalyst (Mg/Zr-1.0) usage. Reaction conditions: 1 mmol glucose, 6 mL H_2O, 80 °C.

Figure 11 examines the effect of substrate concentration on the reaction. The increase in the amount of glucose resulted in a decrease in glucose conversion from 62% to about 40%, which may be due to the fixed amount of catalyst (20 mg), the number of active centers was fixed and the overloaded glucose molecules were not able to participate in the reaction. As can be seen in Figure 11b, the Mg/Zr-1.0-based catalytic system was able to maintain more than 30% fructose yield at a lower substrate concentration system, and when the glucose concentration was enhanced to 10% or more, the fructose yield dropped to about 25%.

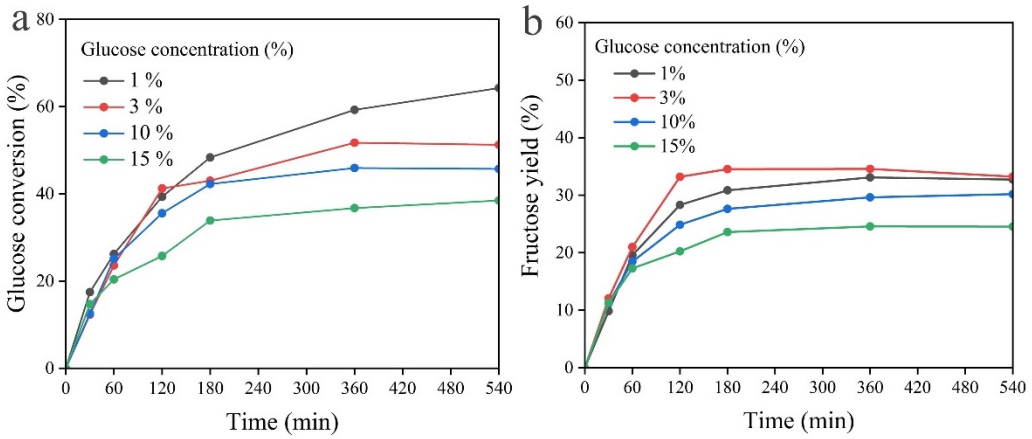

Figure 11. Time-based glucose conversion (**a**) and fructose yield (**b**) of the reaction process at different glucose concentrations. Reaction conditions: 1 mmol glucose, 6 mL H_2O, 80 °C.

In this study, the Mg/Zr-1.0 catalyst was employed to achieve the highest fructose yield of 34.6% from glucose at 80 °C, accompanied by 80.5% selectivity. Comparisons

were drawn with other multiphase catalysts reported in the literature. As illustrated in Table 4, the fructose yields achieved with Mg/Zr-1.0, synthesized herein, surpassed those of the majority of solid catalysts tested under similar conditions in aqueous glucose conversion. Furthermore, our catalyst demonstrated both higher fructose yields and selectivities compared to MgO catalysts derived from calcined magnesite. Notably, these results were accomplished under mild reaction conditions, specifically 80 °C for 120 min. The superior catalytic performance of Mg/Zr-1.0 is attributed to the strategic incorporation of ZrO_2, which effectively modulates the catalyst's basicity distribution.

Table 4. Isomerization of glucose with different heterogeneous catalysts in water.

Catalyst	Reaction Conditions	Glucose Concentration. (wt%)	Fructose Yield. (%)	Fructose Selectivity (%)	Ref.
Al_2O_3	120 °C, 30 min	0.10	27.1	45.6	[50]
CaO/ZrO_2	140 °C, 15 min	0.10	25.0	86.0	[21]
10%MgO/NaY	100 °C, 2 h	2.50	33.8	67.3	[51]
SiO_2-N800	80 °C, 3 h	0.01	22.8	91.3	[52]
MgO/ZrO_2	95 °C, 6 h	3.00	33.0	74.0	[24]
MgO-biochar	100 °C, 30 min	1.00	28.0	34.0	[53]
MgO	90 °C, 45 min	4.00	33.4	75.8	[23]
MgO	80 °C, 2 h	3.00	27.1	66.3	This work
Mg/Zr-1.0	80 °C, 2 h	3.00	34.6	80.5	This work

2.4. Effect of Solvents on Reaction

Polar solvents, such as alcohols, have been reported in the literature to stabilize transition state molecules of glucose, thus further increasing the productivity of fructose from glucose isomerization [54]. Therefore, alcohols have been added to the reaction medium to enhance product selectivity by regulating side reactions. For example, Saravanamurugan et al. proposed a method to promote the isomerization of glucose in a two-step reaction between alcohol and water, achieving a 55% fructose yield (120 °C, 2 h) [55]. In the present work, different alcohols (methanol, ethanol and n-butanol) were added to the aqueous medium to examine the effect of solvents on the reactivity. As shown in Figure 12, in the presence of alcohol, the conversion of glucose decreases sharply, as does the selectivity of fructose. It may be due to the lower solubility of glucose in polar protonating organic solvents at lower reaction temperatures (80 °C), resulting in a slower reaction rate, which reduces the conversion of glucose [56]. In summary, water as a medium facilitates the glucose isomerization fructose reaction.

2.5. Plausible Mechanism of Glucose Isomerization over Mg/Zr-1.0

At present, two acknowledged mechanisms exist for the isomerization of glucose to fructose. One involves the Lewis acid-catalyzed intramolecular hydride transfer mechanism of glucose, while the other entails intramolecular proton transfer (from C2 to O5), resulting in the formation of the enediol key intermediate subsequent to the base-catalyzed ring opening of the glucose molecule [14]. In the present study, based on FTIR spectroscopy and other characterizations, it is known that the Mg/Zr-1.0 catalyst is a heterogeneous base catalyst with moderately to weakly basic active sites, and the reaction follows the principle reported by de Bruyn et al. Water molecules adsorbed on the surface of the Mg/Zr-1.0 catalyst dissociate and form stable hydroxyl groups on the surface of MgO, which is negatively charged [57]. As a result, glucose undergoes deprotonation at the C2 position when it comes into contact with the catalyst surface, forming an enol intermediate, which enables the catalytic isomerization of fructose by the LdB-AVE mechanism (Scheme 1) [18,23].

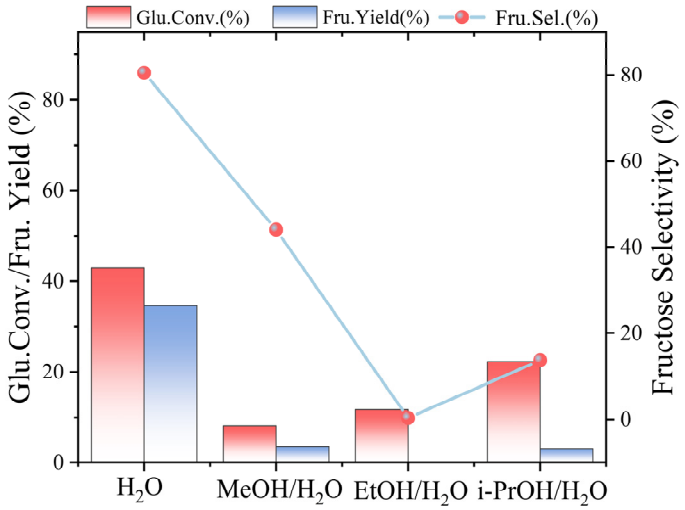

Figure 12. Effect of solvent on glucose isomerization. Reaction conditions: 1 mmol Glucose, 20 mg catalysts, alcohol/H_2O (1:1, *v*:*v*), 2 h, 80 °C.

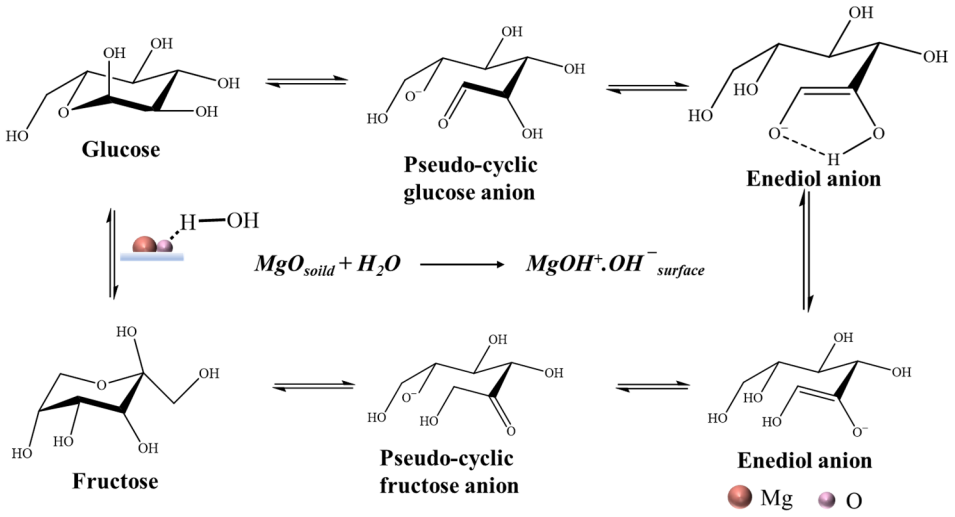

Scheme 1. Proposed mechanism for glucose–fructose isomerization over Mg/Zr-1.0 catalysts.

2.6. Recyclability Test of Mg/Zr-1.0

The stability of the catalyst was further investigated through the recycling tests involving MgO and Mg/Zr-1.0, with the results depicted in Figure 13. The fresh Mg/Zr-1.0 catalyst exhibited substantially improved fructose yield and selectivity over MgO. After two cycles, fructose yield decreased from 34.55% to 20.50% over the Mg/Zr-1.0 catalyst, while a pronounced decrease in fructose yield (from 29.98% to 11.25%) was observed over MgO. Surprisingly, Mg/Zr-1.0 maintained good fructose selectivity (80%) during the cycling test, whereas MgO only offered about 50% fructose selectivity in the cycling test. We further explored the reasons for the decrease in fructose yield. Figure 14 shows the XRD spectra and CO_2-TPD profiles of the pristine and spent Mg/Zr-1.0 catalysts. It can be seen that the intensity of the diffraction peaks corresponding to magnesium oxide is significantly reduced, and the total basic sites are reduced by 77.7 μmol/g. The magnesium leaching of Mg/Zr-1.0 with MgO was examined by inductively coupled plasma atomic emission spectroscopy. The results showed that after two cycles, the cumulative leaching rate of magnesium ions in Mg/Zr-1.0 was only 5.54% (Table 5), and no significant leaching of zirconium ions (less than 1 ppm) was detected, whereas the magnesium leaching rate in MgO was as high as 19.6%. This may explain the greater declines in MgO-catalyzed fructose yields in the cycle. According to the literature, the leaching of MgO may be induced

by the interaction between MgO and organic acids such as acetic, lactic and formic acids, originating from glucose or fructose [23]. Future efforts are thus needed to improve the stability of Mg-based catalysts for glucose isomerization.

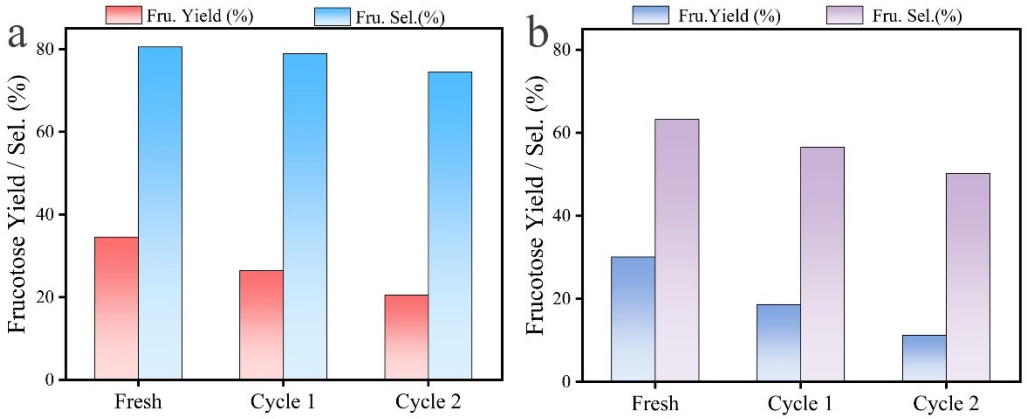

Figure 13. Reusability test of Mg/Zr-1.0 (**a**) and MgO (**b**). Reaction conditions: 1 mmol glucose, 6 mL H_2O, 80 °C, 3 h.

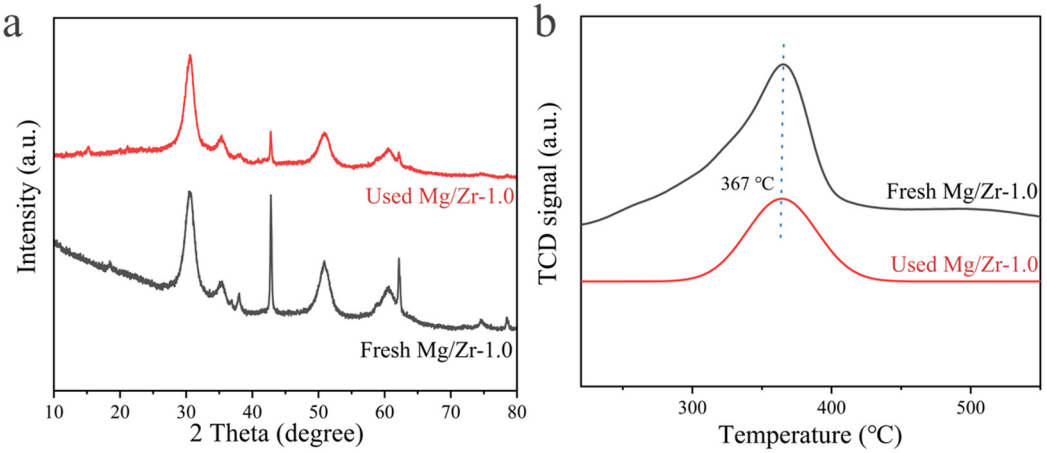

Figure 14. XRD pattern (**a**) and CO_2-TPD profiles (**b**) of fresh Mg/Zr-1.0 and after use.

Table 5. The leaching of magnesium on Mg/Zr-1.0 and MgO, as well as the specific surface area and alkaline sites of pristine and recovered Mg/Zr-1.0 (100 mg), after consecutive run 3 h at 80 °C.

Catalyst	Cycle	Cumulative Leaching Rate of Mg^{2+} (%) [a]	Specific Surface Area [b], (m^2/g)	Basic Sites (μmol/g) [c]
Mg/Zr-1.0	0	0.00	49.6	325.9
Mg/Zr-1.0	1	5.46	--	--
Mg/Zr-1.0	2	5.54	49.8	248.2
MgO	0	0.00	31.6	528.6
MgO	1	17.5	--	--
MgO	2	19.6	31.4	256.2

[a] Cumulative percentage of Mg removed considering their initial amount on each sample. [b] Determined by N_2 adsorption isotherm. [c] Estimated by the CO_2-TPD profiles.

3. Materials and Methods

3.1. Raw Materials

Magnesium nitrate (Mg $(NO_3)_2 \cdot 6H_2O$, 99%) was purchased from Xilong Chemical Co., Ltd. (Shantou, China), glucose (98%) and fructose (98%) were provided by Sinopharm Group Chemical Reagent Co., Ltd. (Shanghai, China), and zirconium nitroxide (ZrO

$(NO_3)_2{\cdot}xH_2O$, 99%) was obtained from Shanghai Aladdin Biochemical Technology Co. (Shanghai, China). All chemicals were utilized in their original state without undergoing additional purification processes.

3.2. Catalyst Preparation

MgO/ZrO_2 composite oxides with different Mg/Zr molar ratios (0.5, 1.0, and 2.0) were prepared by a facile milling–calcination method. The specific steps were as follows: Mg $(NO_3)_2{\cdot}6H_2O$ (0.012 mol), ZrO $(NO_3)_2{\cdot}xH_2O$ (0.012 mol) were mixed in a mortar and ground thoroughly, followed by pyrolysis in a muffle furnace in a static air atmosphere at 450 °C (5 °C/min) for 3 h, obtained a catalyst noted as Mg/Zr-1.0. Similarly, reference is made to zirconium oxide, magnesium oxide, and other bimetallic mixed oxides prepared in a similar way using their respective nitrates with the same nomenclature.

3.3. Catalyst Characterization

X-ray diffraction (XRD) patterns were collected using a Rigaku Ultima IV diffractometer (Akishima, Japan), and X-ray diffraction was carried out in the scanning range of 10–90° (10° min^{-1}) using Cu Kα as the ray source (40 kV, 30 mA) to study the catalyst lattice structure. Physical property parameters were determined and calculated using a physical adsorption meter model ASAP 2020 HD88 from Micromeritics (Norcross, GA, USA). The samples were degassed at 200 °C under vacuum for 6 h prior to N_2 adsorption and desorption analyses. The morphology and elemental distribution of the catalyst surface were recorded by field emission scanning electron microscopy (SEM) coupled with energy-dispersive X-rays (EDX) (Hitaihi, Tokyo, Japan) under an accelerating voltage of 15 kV. Infrared spectra were recorded on the Nicolet Is5 spectrometer (Thermo Fisher Scientific, Waltham, MA, USA). Determination of metal elements in catalysts using Thermo Scientific iCAP 7200 inductively coupled plasma spectrometer.

The basicity of the catalysts was assessed via programmed thermal desorption of carbon dioxide (CO_2-TPD) employing a Micromeritics AutoChem II 2920 fully automated chemisorption instrument. The test procedure was as follows: the samples were preprocessed in a helium atmosphere at 200 °C for 0.5 h, and when the samples were cooled down to 50 °C, the samples were adsorbed by passing through a 10% He/CO_2 gas mixture for 0.5 h. The samples were then purged under He atmosphere (30 mL/min) for 1 h to remove the adsorbed CO_2 on the catalyst surface and finally heated up to 800 °C at an increasing rate of 10 °C/min, and the CO_2-TPD spectra of the samples were recorded during the heating process.

3.4. Glucose Isomerization Experiment

The catalytic reaction took place within a 25 mL closed reactor. In a typical process, 1 mmol of glucose, 20 mg of catalyst (substrate to catalyst mass ratio of 9) and water (6 mL) were added to a 25 mL reactor. It was then heated to 80 °C in an oil bath and stirred with a magnetic bar at 500 rpm. Following a designated reaction period, the reaction vessel was promptly cooled using cold water to rapidly halt the chemical process. The time-based progress of the reaction was monitored by periodically sampling an aliquot (~0.1 mL) of the reaction mixture. This mixture was filtered through a 0.25 mm PES filter membrane (Stronger, Beijing, China) and subsequently analyzed using High-Performance Liquid Chromatography, which was equipped with a Bio-Rad Aminex HPX-87H Organic Acid Column and a refractive index (RI) detector (Hercules, CA, USA). The mobile phase consisted of 5 mM sulfuric acid flowing at a rate of 0.6 mL/min while the column temperature was maintained at 60 °C. Fructose yield and selectivity were assessed utilizing suitable response factors obtained from multipoint calibration curves. Glucose conversion, as well as fructose yield and selectivity, were computed according to the following equations:

$$\text{Glucose convertion rate} = \left(1 - \frac{\text{Molar amount of glucose in the product}}{\text{Initial molar amount of glucose}}\right) \times 100\%$$

$$\text{Fructose yield} = \frac{\text{Molar amount of fructose in the product}}{\text{Initial molar amount of glucose}} \times 100\%$$

$$\text{Fructose selectivity} = \frac{\text{Fructose yield}}{\text{Glucose convertion rate}} \times 100\%$$

The catalyst recovery performance was evaluated for continuous reactions. Following a 3 h reaction period, the catalyst was retrieved via thermal filtration, rinsed with water, and subsequently reused in the subsequent reaction without undergoing any reactivation process.

4. Conclusions

In this contribution, solid base catalysts obtained by simple grinding and calcination of the metal-mixed salts containing magnesium nitrate and zirconium nitroxide can be used for the isomerization of glucose to fructose in water. A Mg/Zr molar ratio of 1 in Mg/Zr-1.0 resulted in a fructose yield of 34.55%, with a selectivity close to 80.52%. Catalyst characterizations indicated that the introduction of ZrO_2 facilitated the transformation of strongly basic sites over Mg/Zr composite oxides to moderately and weakly basic sites, resulting in a decrease in the total number of basic sites. Therefore, the side reactions of fructose were probably inhibited, guaranteeing a desirable fructose selectivity for glucose isomerization. In addition, the incorporation of ZrO_2 largely improved the catalytic stability of Mg/Zr-1.0 by the suppression of MgO leaching.

Author Contributions: Conceptualization, X.Z.; formal analysis, X.Z.; data curation, X.Z.; writing—original draft preparation, X.Z.; writing—review and editing, X.T.; supervision, X.T.; project administration, X.T. All authors have read and agreed to the published version of the manuscript.

Funding: This research received no external funding.

Data Availability Statement: Data are contained within the article.

Conflicts of Interest: The authors declare no conflicts of interest.

References

1. Tshikovhi, A.; Motaung, T.E. Technologies and innovations for biomass energy production. *Sustainability* **2023**, *15*, 12121. [CrossRef]
2. Queneau, Y.; Han, B. Biomass: Renewable carbon resource for chemical and energy industry. *Innovation* **2022**, *3*, 100184. [CrossRef]
3. Zhu, J.; Pan, X. Efficient sugar production from plant biomass: Current status, challenges, and future directions. *Renew. Sustain. Energy Rev.* **2022**, *164*, 112583. [CrossRef]
4. Wang, Z.; Bhattacharyya, S.; Vlachos, D.G. Extraction of furfural and furfural/5-hydroxymethylfurfural from mixed lignocellulosic biomass-derived feedstocks. *ACS Sustain. Chem. Eng.* **2021**, *9*, 7489–7498. [CrossRef]
5. Zhang, Z.-H.; Sun, Z.; Yuan, T.-Q. Recent advances in the catalytic upgrading of biomass platform chemicals via hydrotalcite-derived metal catalysts. *Trans. Tianjin Univ.* **2022**, *28*, 89–111. [CrossRef]
6. Liu, H.; Jia, W.; Yu, X.; Tang, X.; Zeng, X.; Sun, Y.; Lei, T.; Fang, H.; Li, T.; Lin, L. Vitamin C-assisted synthesized Mn–Co oxides with improved oxygen vacancy concentration: Boosting lattice oxygen activity for the air-oxidation of 5-(hydroxymethyl)Furfural. *ACS Catal.* **2021**, *11*, 7828–7844. [CrossRef]
7. Han, J.; Wan, J.; Wang, Y.; Wang, L.; Li, C.; Mao, Y.; Ni, L. Recyclable soluble-insoluble upper critical solution temperature-type poly(methacrylamide-Co-acrylic acid)–cellulase biocatalyst for hydrolysis of cellulose into glucose. *ACS Sustain. Chem. Eng.* **2018**, *6*, 7779–7788. [CrossRef]
8. Tang, X.; Zuo, M.; Li, Z.; Liu, H.; Xiong, C.; Zeng, X.; Sun, Y.; Hu, L.; Liu, S.; Lei, T.; et al. Green processing of lignocellulosic biomass and its derivatives in deep eutectic solvents. *ChemSusChem* **2017**, *10*, 2696–2706. [CrossRef]
9. Ståhlberg, T.; Sergio, R.-R.; Fristrup, P.; Riisager, A. Metal-free dehydration of glucose to 5-(hydroxymethyl)furfural in ionic liquids with boric acid as a promoter. *Chem. A Eur. J.* **2011**, *17*, 1456–1464. [CrossRef]
10. Li, H.; Riisager, A.; Saravanamurugan, S.; Pandey, A.; Sangwan, R.S.; Yang, S.; Luque, R. Carbon-increasing catalytic strategies for upgrading biomass into energy-intensive fuels and chemicals. *ACS Catal.* **2017**, *8*, 148–187. [CrossRef]
11. Liu, Y.; Qiu, Y.; Jia, W.; Li, Z.; Zhang, J.; Sun, Y.; Tang, X.; Zeng, X.; Lin, L. Solvent-mediated Zr-based coordination polymer with tunable acid properties for the dehydration of fructose and catalytic transfer hydrogenation of 5-hydroxymethylfurfural. *Mol. Catal.* **2022**, *524*, 112253. [CrossRef]
12. Nam, K.H. Glucose isomerase: Functions, structures, and applications. *Appl. Sci.* **2022**, *12*, 428. [CrossRef]

13. Gao, D.-M.; Zhang, X.; Liu, H.; Fujino, H.; Lei, T.; Sun, F.; Zhu, J.; Huhe, T. Critical approaches in the catalytic transformation of sugar isomerization and epimerization after fischer-history, challenges, and prospects. *Green Energy Environ.* **2023**, *9*, 435–453. [CrossRef]
14. Li, H.; Yang, S.; Saravanamurugan, S.; Riisager, A. Glucose isomerization by enzymes and chemo-catalysts: Status and current advances. *ACS Catal.* **2017**, *7*, 3010–3029. [CrossRef]
15. Liu, C.; Carraher, J.M.; Swedberg, J.L.; Herndon, C.R.; Fleitman, C.N.; Tessonnier, J.-P. Selective base-catalyzed isomerization of glucose to fructose. *ACS Catal.* **2014**, *4*, 4295–4298. [CrossRef]
16. Hou, Q.; Rehman, M.L.U.; Bai, X.; Xie, C.; Lai, R.; Qian, H.; Xia, T.; Yu, G.; Tang, Y.; Xie, H.; et al. Incorporation of MgO into nitrogen-doped carbon to regulate adsorption for near-equilibrium isomerization of glucose into fructose in water. *Appl. Catal. B Environ.* **2024**, *342*, 123443. [CrossRef]
17. Zhao, C.; Zhu, N.; Qiu, G.; Zhang, M.; Tian, H. Effective synergistic hafnium-aluminum bimetallic oxides catalysts for the synthesis of 5-hydroxymethylfurfural from glucose and fructose. *Mol. Catal.* **2023**, *547*, 113407. [CrossRef]
18. Marianou, A.A.; Michailof, C.M.; Pineda, A.; Iliopoulou, E.F.; Triantafyllidis, K.S.; Lappas, A.A. Glucose to fructose isomerization in aqueous media over homogeneous and heterogeneous catalysts. *ChemCatChem* **2016**, *8*, 1100–1110. [CrossRef]
19. Tang, J.; Guo, X.; Zhu, L.; Hu, C. Mechanistic study of glucose-to-fructose isomerization in water catalyzed by $[Al(Oh)_2(Aq)]^+$. *ACS Catal.* **2015**, *5*, 5097–5103. [CrossRef]
20. Drabo, P.; Fischer, M.; Toussaint, V.; Flecken, F.; Palkovits, R.; Delidovich, I. What are the catalytically active species for aqueous-phase isomerization of d-glucose into d-fructose in the presence of alkaline earth metal (hydr)oxides? *J. Catal.* **2021**, *402*, 315–324. [CrossRef]
21. Kitajima, H.; Higashino, Y.; Matsuda, S.; Zhong, H.; Watanabe, M.; Aida, T.M.; Smith, R.L. Isomerization of glucose at hydrothermal condition with TiO_2, ZrO_2, CaO-doped ZrO_2 or TiO_2-doped ZrO_2. *Catal. Today* **2016**, *274*, 67–72. [CrossRef]
22. Tamura, M.; Kishi, R.; Nakayama, A.; Nakagawa, Y.; Hasegawa, J.; Tomishige, K. Formation of a new, strongly basic nitrogen anion by metal oxide modification. *J. Am. Chem. Soc.* **2017**, *139*, 11857–11867. [CrossRef] [PubMed]
23. Marianou, A.A.; Michailof, C.M.; Ipsakis, D.K.; Karakoulia, S.A.; Kalogiannis, K.G.; Yiannoulakis, H.; Triantafyllidis, K.S.; Lappas, A.A. Isomerization of glucose into fructose over natural and synthetic MgO catalysts. *ACS Sustain. Chem. Eng.* **2018**, *6*, 16459–16470. [CrossRef]
24. Rabee, A.I.M.; Le, S.D.; Nishimura, S. MgO-ZrO_2 mixed oxides as effective and reusable base catalysts for glucose isomerization into fructose in aqueous media. *Chem. Asian J.* **2019**, *15*, 294–300. [CrossRef] [PubMed]
25. Mahala, S.; Arumugam, S.M.; Kumar, S.; Devia, B.; Elumalai, S. Tuning of MgO's base characteristics by blending it with amphoteric ZnO facilitating the selective glucose isomerization to fructose for bioenergy development. *Nanoscale Adv.* **2023**, *5*, 2470–2486. [CrossRef]
26. Watanabe, M.; Aizawa, Y.; Iida, T.; Nishimura, R.; Inomata, H. Catalytic glucose and fructose conversions with TiO_2 and ZrO_2 in water at 473k: Relationship between reactivity and acid-base property determined by TPD measurement. *Appl. Catal. A Gen.* **2005**, *295*, 150–156. [CrossRef]
27. Provenzi, C.; Collares, F.M.; Cuppini, M.; Samuel, S.M.W.; Alves, A.K.; Bergmann, C.P.; Leitune, V.C.B. Effect of nanostructured zirconium dioxide incorporation in an experimental adhesive resin. *Clin. Oral Investig.* **2018**, *22*, 2209–2218. [CrossRef] [PubMed]
28. Arumugam, S.M.; Singh, D.; Mahala, S.; Devi, B.; Kumar, S.; Jakhu, S.; Elumalai, S. MgO/CaO nanocomposite facilitates economical production of d-fructose and d-allulose using glucose and its response prediction using a DNN model. *Ind. Eng. Chem. Res.* **2022**, *61*, 2524–2537. [CrossRef]
29. Limo, M.J.; Sola-Rabada, A.; Boix, E.; Thota, V.; Westcott, Z.C.; Puddu, V.; Perry, C.C. Interactions between metal oxides and biomolecules: From fundamental understanding to applications. *Chem. Rev.* **2018**, *118*, 11118–11193. [CrossRef]
30. Rao, L.S.; Rao, T.V.; Naheed, S.; Rao, P.V. Structural and optical properties of zinc magnesium oxide nanoparticles synthesized by chemical co-precipitation. *Mater. Chem. Phys.* **2018**, *203*, 133–140. [CrossRef]
31. Oishi, M.; Tsutsumi, Y.; Chen, P.; Ashida, M.; Doi, H.; Hanawa, T. Surface changes of yttria-stabilized zirconia in water and hanks solution characterized using XPS. *Surf. Interface Anal.* **2018**, *50*, 587–591. [CrossRef]
32. Wang, Y.; Chen, Y.; Liu, C.; Yu, F.; Chi, Y.; Hu, C. The effect of magnesium oxide morphology on adsorption of U(VI) from aqueous solution. *Chem. Eng. J.* **2017**, *316*, 936–950. [CrossRef]
33. Guo, W.; Lin, H.; Zhu, H.; Lei, M.; Feng, J. Preparation and application of magnesium oxide nanoparticles for superiorly fluoride removal. *J. Alloys Compd.* **2023**, *960*, 170935. [CrossRef]
34. Navas, M.B.; Bolla, P.A.; Lick, I.D.; Casella, M.L.; Ruggera, J.F. Transesterification of soybean oil to biodiesel by using heterogeneous basic catalysts. *Ind. Eng. Chem. Res.* **2006**, *45*, 3009–3014.
35. Yamaguchi, T.; Morita, T.; Salama, T.M.; Tanabe, K. Surface properties of ZrO_2 dispersed on SiO_2. *Catal. Lett.* **1990**, *4*, 1–6. [CrossRef]
36. Abinaya, S.; Kavitha, H.P. Magnesium oxide nanoparticles: Effective antilarvicidal and antibacterial agents. *ACS Omega* **2023**, *8*, 5225–5233.
37. Chizallet, C.; Costentin, G.; Lauron-Pernot, H.; Krafft, J.; Bazin, P.; Saussey, J.; Delbecq, F.; Sautet, P.; Che, M. Role of hydroxyl groups in the basic reactivity of MgO: A theoretical and experimental study. *Oil Gas Sci. Technol. Rev. L'IFP* **2007**, *61*, 479–488. [CrossRef]

38. Debecker, D.P.; Gaigneaux, E.M.; Busca, G. Exploring, tuning, and exploiting the basicity of hydrotalcites for applications in heterogeneous catalysis. *Chem. A Eur. J.* **2009**, *15*, 3920–3935. [CrossRef]
39. Cornu, D.; Guesmi, H.; Krafft, J.-M.; Lauron-Pernot, H. Lewis acido-basic interactions between CO_2 and MgO surface: DFT and DRIFT approaches. *J. Phys. Chem. C* **2012**, *116*, 6645–6654. [CrossRef]
40. Delidovich, I.; Palkovits, R. Structure-performance correlations of Mg-Al hydrotalcite catalysts for the isomerization of glucose into fructose. *J. Catal.* **2015**, *327*, 1–9. [CrossRef]
41. Delidovich, I.; Palkovits, R. Catalytic activity and stability of hydrophobic Mg-Al hydrotalcites in the continuous aqueous-phase isomerization of glucose into fructose. *Catal. Sci. Technol.* **2014**, *4*, 4322–4329. [CrossRef]
42. Yang, Q.; Lan, W.; Runge, T. Salt-promoted glucose aqueous isomerization catalyzed by heterogeneous organic base. *ACS Sustain. Chem. Eng.* **2016**, *4*, 4850–4858. [CrossRef]
43. Lin, C.; Shi, Y.; Xu, L.; Wang, Z.; Zhao, L.; Wu, H.; Cao, F.; Wei, P. Insight into the alkaline earth metal salt promotion for alkali-catalyzed glucose isomerization. *Catal. Sci. Technol.* **2024**, *14*, 718–727. [CrossRef]
44. Tang, J.; Zhu, L.; Fu, X.; Dai, J.; Guo, X.; Hu, C. Insights into the kinetics and reaction network of aluminum chloride-catalyzed conversion of glucose in NaCl–H_2O/THF biphasic system. *ACS Catal.* **2016**, *7*, 256–266. [CrossRef]
45. Knill, C.J.; Kennedy, J.F. Degradation of cellulose under alkaline conditions. *Carbohydr. Polym.* **2003**, *51*, 281–300. [CrossRef]
46. Yang, B.Y.; Montgomery, R. Alkaline degradation of glucose: Effect of initial concentration of reactants. *Carbohydr. Res.* **1996**, *280*, 27–45. [CrossRef]
47. Sun, Y.; Ma, S.; Du, Y.; Yuan, L.; Wang, S.; Yang, J.; Deng, F.; Xiao, F.-S. Solvent-free preparation of nanosized sulfated zirconia with brønsted acidic sites from a simple calcination. *J. Phys. Chem. B* **2005**, *109*, 2567–2572. [CrossRef] [PubMed]
48. Li, C.; Wang, Y.; Zhang, Y.; Wang, M.; Sun, X.; Cui, H.; Xie, Y. Isomerization kinetics of glucose to fructose in aqueous solution with magnesium-aluminum hydrotalcites. *ChemistrySelect* **2020**, *5*, 270–279. [CrossRef]
49. Li, B.; Jiang, H.; Zhao, X.; Pei, Z.; Zhang, Q. Enhanced conversion of glucose to fructose over naturalattapulgite catalyst promoted by CeO_2 in water. *ChemistrySelect* **2020**, *5*, 14971–14977. [CrossRef]
50. Steinbach, D.; Klier, A.; Kruse, A.; Sauer, J.; Wild, S.; Zanker, M. Isomerization of glucose to fructose in hydrolysates from lignocellulosic biomass using hydrotalcite. *Processes* **2020**, *8*, 644. [CrossRef]
51. Li, B.; Li, L.; Dong, Y.; Zhang, Q.; Weng, W.; Wan, H. Glucose isomerization into fructose Catalyzed by MgO/NaY Catalyst. *Chin. J. Chem. Phys.* **2018**, *31*, 203–210. [CrossRef]
52. Otomo, R.; Fujimoto, M.; Nagao, M.; Kamiya, Y. Ammonia-treated metal oxides as base catalysts for selective isomerization of glucose in water. *Mol. Catal.* **2019**, *475*, 110479. [CrossRef]
53. Chen, S.S.; Cao, Y.; Tsang, D.C.W.; Tessonnier, J.-P.; Shang, J.; Hou, D.; Shen, Z.; Zhang, S.; Ok, Y.S.; Wu, K.C.W. Effective dispersion of MgO nanostructure on biochar support as a basic catalyst for glucose isomerization. *ACS Sustain. Chem. Eng.* **2020**, *8*, 6990–7001. [CrossRef]
54. Yabushita, M.; Shibayama, N.; Nakajima, K.; Fukuoka, A. Selective glucose-to-fructose isomerization in ethanol catalyzed by hydrotalcites. *ACS Catal.* **2019**, *9*, 2101–2109. [CrossRef]
55. Saravanamurugan, S.; Paniagua, M.; Melero, J.A.; Riisager, A. Efficient isomerization of glucose to fructose over zeolites in consecutive reactions in alcohol and aqueous media. *J. Am. Chem. Soc.* **2013**, *135*, 5246–5249. [CrossRef]
56. Gao, D.-M.; Kobayashi, T.; Adachi, S. Promotion or suppression of glucose isomerization in subcritical aqueous straight- and branched-chain alcohols. *Biosci. Biotechnol. Biochem.* **2015**, *79*, 470–474. [CrossRef]
57. Li, B.; Chen, H.; Feng, J.; Ma, Q.; Chen, J.; Ren, B.; Yin, S.; Jiang, P. First principles calculation of adsorption of water on MgO (100) plane. *Materials* **2023**, *16*, 2100. [CrossRef]